Jurnal Elektronika dan Telekomunikasi (JET), Vol. 25, No. 1, August 2025, pp. 1-8
Accredited by KEMDIKBUDRISTEK, Decree No: **158/E/KPT/2021**
doi: 10.55981/jet.703

Comparative Analysis of Charge Recombination Dynamics in Dye-Sensitized Solar Cells with Different Counter Electrodes

Evi Nur Azizah[a], Nunik Nurhayati[b], Lalu Jihad Al Jazeera[c], Lia Yuliantini[b], Mohammad Hatta[d], Tahta Amrillah[c], Natalita Maulani Nursam[b], Yuliar Firdaus[b,*]

[a]Department of Physics, Faculty of Mathematics and Natural Science Education
Universitas Pendidikan Indonesia
Jl. Dr. Setiabudi, Isola, Sukasari
Bandung, Indonesia
[b]Research Center for Electronics
National Research and Innovation Agency (BRIN)
KST Samaun Samadikun, Jl. Sangkuriang, Dago
Bandung, Indonesia
[c]Nanotechnology Engineering, Faculty of Advanced Technology and Multidiscipline
Universitas Airlangga
Campus MERR, Mulyorejo
Surabaya, Indonesia
[d]Department of Physics, Faculty of Mathematics and Natural Sciences
Universitas Indonesia
Jl. Prof. Dr. Mahar Mardjono, Kampus UI Depok
Depok, Indonesia

Abstract

Counter electrodes are essential in dye-sensitized solar cells (DSSCs) for facilitating charge transfer and catalyzing the regeneration of the electrolyte, impacting overall efficiency. Common counter-electrode materials include platinum (Pt), poly(3,4-ethylenedioxythiophene): polystyrene sulfonate (PEDOT:PSS), and graphene, each with distinct advantages and challenges. Pt, a traditional choice, offers excellent catalytic activity but is limited by its high cost and scarcity. PEDOT:PSS, a conductive polymer, is cost-effective and easily deposited but often suffers from high recombination losses and lower efficiency. Graphene, known for its high conductivity and large surface area, is emerging as a promising alternative. However, a lack of comparative studies on how different counter-electrode materials influence recombination dynamics limits the understanding needed for optimizing DSSC performance. This study addresses this gap by examining Pt, graphene, and PEDOT:PSS-based counter electrodes, analyzing their effects on charge transfer, recombination behavior, and efficiency through current density-voltage (*J-V*) measurements, charge extraction, and transient photocurrent (TPC) as well as transient photovoltage (TPV) analyses. Graphene-based DSSCs show superior performance, achieving the highest photocurrent density and power conversion efficiency up to 5.12% at an intensity equivalent to 1 sun (100 $mWcm^{-2}$) due to enhanced charge extraction and minimized recombination. TPC data reveal that graphene supports faster charge transport, while TPV analysis shows longer electron lifetimes than PEDOT:PSS-based DSSCs. In contrast, PEDOT:PSS-based DSSCs exhibit high recombination losses, lower photocurrent, and s-shaped *J-V* curves, indicating high resistance of limited charge transfer efficiency. These findings highlight graphene's potential as an optimal counter-electrode material for efficient, high-performance DSSCs.

Keywords: Dye-sensitized solar cells, counter electrodes, recombination dynamics, graphene electrodes, charge extraction, PEDOT:PSS.

I. INTRODUCTION

Dye-sensitized solar cells (DSSCs) have attracted significant attention as a promising photovoltaic technology due to their relatively low cost, ease of fabrication, and potential for different applications [1-3]. Central to DSSC performance is the efficiency of the counter electrode, which plays a vital role in facilitating charge transfer and catalyzing the regeneration of the redox mediator in the electrolyte [4]. Platinum (Pt) is typically used as the counter electrode material due to its high catalytic activity and stability. However, its high cost and scarcity have driven research efforts toward identifying alternative materials that can deliver comparable or superior performance [5].

Graphene and poly(3,4-ethylenedioxythiophene): polystyrene sulfonate (PEDOT:PSS) have emerged as promising counter-electrode materials [5]. Graphene, defined as one single atomic thick layer of the mineral graphite, with its high electrical conductivity [6], high specific area [7], and exceptional catalytic properties [8], has shown a potential to enhance charge transfer and minimize recombination losses in DSSCs [5]. PEDOT, a conductive polymer with good transparency and processability, has also been investigated as a low-cost

* Corresponding Author.
Email: yuliar.firdaus@brin.go.id
Received: November 19, 2024 ; Revised : December 17, 2024
Accepted: December 24, 2024 ; Published: August 31, 2025

alternative. Compared to PEDOT:PSS, PEDOT film prepared by electrochemical deposition typically results in a highly conductive, dense, and smooth film, which can improve charge transport and catalyze the reaction of I^-/I_3^- at the electrode [9]. The electrochemical-based polymerization of PEDOT film has been used as a counter electrode in the currently best-performing DSSCs (15.2% under a standard air mass of 1.5G) [10]. The PEDOT:PSS films are also commonly used as counter electrodes in DSSCs [11-14]. The application of PEDOT:PSS could reduce production costs and simplify fabrication, typically through spin coating. However, the power conversion efficiency of the PEDOT: PSS-based DSSCs is relatively low due to its poor catalytic activity for I_3^- reduction and lower conductivity due to the presence of the insulating PSS [13].

Despite numerous efforts to find alternative counter electrodes, comprehensive studies are still needed to compare the recombination dynamics, charge transfer efficiency, and overall photovoltaic performance of DSSCs with various counter electrodes. This research aims to address this gap by systematically evaluating Pt, graphene, and PEDOT:PSS counter electrodes in DSSCs. Using *J-V* measurements under different light intensities, we assess their impact on key parameters such as photocurrent density (J_{SC}), open-circuit voltage (V_{OC}), and power conversion efficiency (PCE). Additionally, charge extraction, transient photovoltage (TPV), and transient photocurrent (TPC) measurements are conducted to gain insight into charge recombination dynamics and charge transport behavior. The TPV and TPC techniques allow for a deeper understanding of the electron lifetime and electron transport time, respectively, helping to identify how each counter-electrode material influences recombination rates and charge extraction efficiency.

Our results show that graphene-based DSSCs achieve the highest J_{SC} and PCE, due to superior charge extraction and minimal recombination. In contrast, PEDOT:PSS-based DSSCs exhibit significant recombination losses, as evidenced by lower J_{SC} values, a pronounced s-shaped *J-V* curve, and high resistive losses at increased light intensities. The findings underscore graphene's potential as a high-performance counter-electrode material in DSSCs and highlight the limitations of PEDOT:PSS regarding charge transfer efficiency and recombination dynamics. This study contributes to the growing body of knowledge on DSSC optimization and provides a comparative foundation for future research on counter-electrode materials, paving the way for more efficient and cost-effective DSSCs.

II. METHODS

A. Material

PT1 Platinum Paste, fluorine-doped tin oxide (FTO) glass substrate, BL-1 blocking layer paste, 18NR-AO active opaque titanium paste**,** ruthenium-based hydrophobic dye Z907 cis-Bis(isothiocyanato)(2,2′-bipyridyl-4,4′-dicarboxylato)(4,4′-di-nonyl-2′-bipyridyl)ruthenium(II)], and iodide-triiodide based liquid high-performance electrolyte (EL-HPE) were purchased from Greatcell Solar. Hydroxyethyl cellulose and titanium tetrachloride ($TiCl_4$) were purchased from Merck. Terpineol, acetone, ethanol, and P25 TiO_2 were purchased from Sigma Aldrich. PEDOT:PSS (AI 4083) was purchased from Ossila. Surlyn thermoplastic sheet was purchased from DuPont. Graphene was purchased from Saidkocc. Subsequently, the graphene powder was processed into graphene paste. The graphene-based paste for the counter electrode was processed by carefully weighing 0.23 g of graphene, adding 300 µL of terpineol, 0.0383 g of TiO_2 (P25), and 0.0383 g of hydroxyethyl cellulose. This combination was meticulously crushed in a mortar for two hours to create a fine, consistent paste. After the paste attained the desired consistency, it was transferred to a 5 mL vial and agitated for 24 h at 500 rpm to increase homogeneity. As binding agents, TiO_2 (P25) and hydroxyethyl cellulose were used to ensure a strong adhesion between the graphene layer and the FTO substrate.

B. Device Fabrication

The DSSCs were fabricated by first cutting the FTO substrates to 1 cm × 1.5 cm. After device assembly, the FTO assigned as counter electrodes were drilled at their top corner side for electrolyte injection. All substrates were cleaned by subsequent steps: ultrasonication in a dilute detergent solution (Teepol), deionized water, acetone, and ethanol for 15 minutes each. Afterward, the photoanodes were prepared initially by screen print blocking layer paste (BL-1) on conductive FTO glass and subsequently annealed at 500°C for 30 minutes. After blocking layer (BL) deposition, an opaque TiO_2 paste was screen-printed with an area of 0.5 cm × 0.5 cm on the BL-coated FTO using a 200T mesh screen printer and dried in the oven at 120°C for 10 mins. Annealing the paste at 500°C for 30 minutes was done after two cycles of screen-printing. After annealing, the substrate was immersed in $TiCl_4$ solution and heated at 70°C for 30 min to expand the surface area of TiO_2 [15]. Furthermore, the substrate was immersed in a dye Z907 solution (6 mg of Z907 dissolved in 30 mL of ethanol) for 24 hours, rinsed with ethanol, and dried at room temperature.

The counter electrodes (CEs) were fabricated with three variations: platinum (Pt)-coated FTO, PEDOT:PSS-coated FTO, and graphene-coated FTO. Pt and graphene-based CEs were prepared using the screen-printing method to form the film with an area of 1 cm^2. Then, the substrates were heated at 120°C for 10 minutes to dry the paste. The screen-printing process was repeated two cycles before annealing the substrates at 450°C for 30 minutes. PEDOT:PSS-based CE was prepared by spin-coating the AI-4083 solution at 3000 rpm on FTO substrates, followed by annealing at 100°C.

The dyed photoanodes were then sandwiched with the counter electrode with Surlyn thermoplastic sealant in between, followed by a hot-pressed process at 130°C and pressure of 0.15 – 0.20 MPa for 30 seconds and injected with an HPE I_3^-/I^- electrolyte solution. The drilled hole for the electrolyte injection was then sealed using Surlyn, and the contact was added with silver conductive ink to improve the contact during the *J-V* measurements.

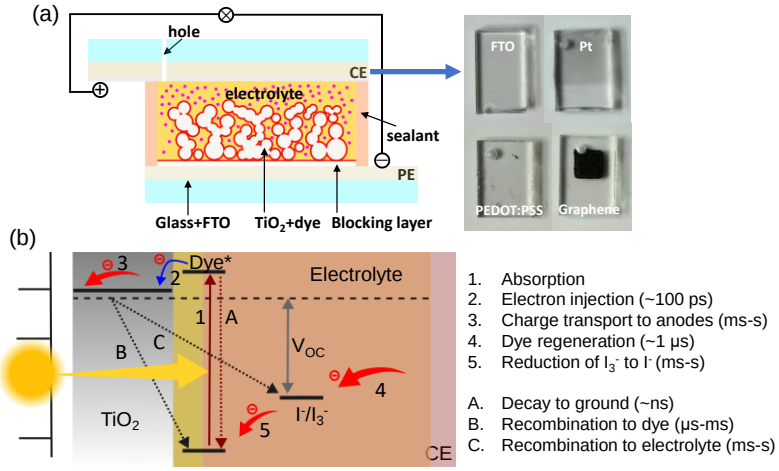

Figure 1. (a) The sandwich structure of DSSCs. (b) The working and losses mechanism diagram of DSSCs.

C. Characterization

1) Scanning Electron Microscopy-Energy Dispersive X-ray (SEM EDX)

Scanning Electron Microscope (SEM) was operated using Jeol JSM-IT300LV with Oxford X-Max EDX.

2) Resistivity Measurement

Resistivity (conductivity) measurements were conducted using Four Point Probe Alessi with Multimeter HP 3468A and DC Current Source 6186C at ambient temperature and pressure. Sheet resistance values were computed using the formula as follows:

$$R_s = V/I \times F_2 \quad (1)$$

R_s is for sheet resistance, V is for voltage, I is for an electrical current, and F_2 is for a geometrical correction factor.

3) UV Reflectance

Ultraviolet-visible (*UV*) reflectance spectra of the counter electrodes were measured in the absorbance and diffuse reflectance mode using a Maya DH-2000 Pro Ocean Optics *UV*-visible spectrophotometer.

4) J-V and Charge Recombination Measurements

The photovoltaic performances and charge recombination measurements (*J-V* vs light-intensity dependent, charge extraction, transient photocurrent (TPC), transient photovoltage (TPV), and voltage decay) were conducted using a Dyenamo Toolbox with a 1 W, 350 mA, 3.2 V electrical specification of LED Seoul Semiconductor Natural White (S42182H) and a Thorlabs PDA200C current amplifier calibrated with a Pyranometer.

III. Results and Discussion

Figure 1(a) depicts the sandwich structure of DSSCs with photoanode (TiO_2 layer on top of FTO), electrolyte, and counter electrode (CE). The counter electrodes using different materials, such as Pt, PEDOT:PSS, and graphene, are shown. As shown in Figure 1b, charge generation in DSSCs briefly starts from the absorption of the light by the dye molecules and electron excitation, injection of the excited electron into the conduction band of the TiO_2, charge transport through the TiO_2 network and to the external circuit, dye regeneration, reduction of I_3^- to I^- as a result of electron transfer from counter electrode. The diagram also shows recombination kinetics in the DSSCs and their timescale.

To illustrate the differences in the morphology of the counter electrodes discussed in this work, SEM SEM characterizations of Pt, PEDOT:PSS, and graphene on FTO were performed. The SEM images are shown in Figure 2. For comparison, the FTO surface (Figure 2(a)) displays a granular structure with relatively uniform grain distribution (average grain sizes ~137 nm). The Pt-coated FTO (Figure 2(b)) shows a similar granular texture to the FTO reference. The grain size is slightly smaller (~120 nm) and dense, indicating that the platinum layer has been successfully deposited on the FTO. The existence of Pt is also confirmed with EDX (energy dispersive X-ray), as shown in Table 1. PEDOT:PSS

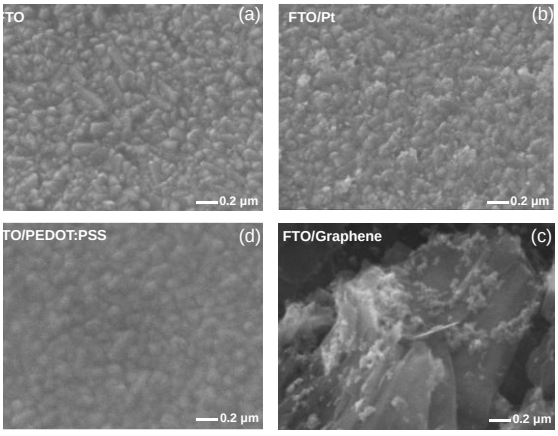

Figure 2. SEM images of (a) FTO, (b) Pt-coated FTO, (c) PEDOT:PSS-coated FTO, and (d) graphene-coated FTO.

TABLE 1
EDX ANALYSIS RESULTS SHOWING ATOMIC PERCENT CONCENTRATIONS OF THE COUNTER ELECTRODES (CES)

CE	% C	% O	% F	% Sn	% Pt
FTO	-	38.45	-	61.55	-
FTO/Pt	-	37.87	-	60.03	2.11
FTO/PEDOT:PSS	4.52	35.24	-	60.24	-
FTO/Graphene	90.19	9.04	0.77	-	-

(Figure 2(c)) shows a smoother, more compact morphology than bare FTO and Pt. Its deposition was confirmed by the increase in the atomic percentage of carbon atoms from the EDX analysis. The graphene-coated FTO (Figure 2(d)) shows a more heterogeneous surface than FTO, Pt, and PEDOT:PSS. The sheet-like structure of graphene is visible, with areas of wrinkling and overlapping. On the surface, some agglomeration also appears. This morphology is advantageous for the graphene counter electrode's electrical conductivity and catalytic performance [16].

One of the requirements for counter electrodes is conductive properties [5]. Resistivity measurements were conducted for all the counter electrodes to check their conductivity properties. Table 2 shows the sheet resistance data of the counter electrodes. Bare FTO glass has a sheet resistance value of 19.1 $\Omega.sq^{-1}$; this value is higher than Pt-coated FTO and PEDOT:PSS-coated FTO, which produces 18.9 $\Omega.sq^{-1}$ and 17.5 $\Omega.sq^{-1}$, respectively, but lower than graphene-coated FTO that has a sheet resistance of 22.8 $\Omega.sq^{-1}$. This means that PEDOT:PSS-coated FTO is the most conductive of all the samples.

Subsequently, the optical properties of the counter electrodes were evaluated. Figure 3(a) shows the optical absorption spectra of Pt and PEDOT:PSS film on FTO. Pt film exhibits absorbance mainly below 350 nm, whereas the PEDOT:PSS film shows absorbance below 250 nm and with a lower overall intensity than the Pt film, which makes higher transmittance of the PEDOT:PSS film than Pt film from the UV to the visible region. Since the graphene film on FTO is opaque, its optical properties are demonstrated through reflectance spectra. As shown in Figure 3(b), the graphene film exhibits higher reflectance than bare FTO across the visible region, which could be important for enhancing light absorption in the photoactive layer [17].

TABLE 2
SHEET RESISTANCE (R_S) DATA OF THE ELECTRODES

CE	Sheet Resistance (R_s) $\Omega.SQ^{-1}$
FTO	19.1
FTO/Pt	18.9
FTO/PEDOT:PSS	17.5
FTO/ Graphene	22.8

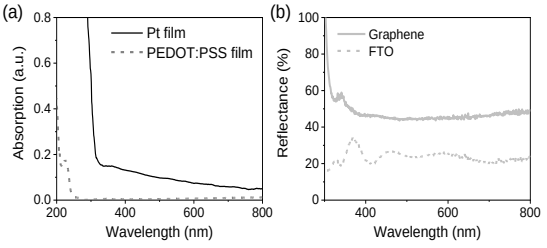

Figure 3. Optical properties of the material for counter electrodes. (a) absorption spectra of Pt and PEDOT:PSS film and (b) reflectance spectra of graphene and FTO.

J-V measurements were conducted under simulated sunlight at an intensity equivalent to 1 sun (around 100 $mW.cm^{-2}$) to evaluate and compare the performance of different counter-electrode materials in DSSCs. The resulting *J-V* curves, shown in Figure 4(a), and the corresponding device data in Table 3 provide insights into the photocurrent density (J_{SC}), charge transfer efficiency, and catalytic activity of graphene, Pt, and PEDOT:PSS-based counter electrodes. Graphene-based DSSC shows the highest average J_{SC} of 14.2 $mA.cm^{-2}$ compared to the Pt-based and PEDOT:PSS-based DSSCs (12.4 and 4.7 $mA.cm^{-2}$, respectively). The graphene-based cell can achieve J_{SC} and PCE up to 15.5 $mA.cm^{-2}$ and 5.23%, respectively (Table 3). This increased J_{SC} suggests that graphene has superior charger transfer and catalytic activity at the counter electrode. As a result, the DSSC with graphene also achieves the highest average power conversion efficiency (PCE) of 4.81%. The DSSC with Pt counter electrode also performs well but shows lower average J_{SC} and average fill-factor (FF) of 49.4% compared to graphene (FF of 53%). PEDOT:PSS shows the poorest performance with average PCE of 0.8% and an s-shape-like *J-V* curve, suggesting higher resistance than the other two counter electrodes. This effect results in the poor current generation and a low average FF of 26.2%, highlighting the limitations of PEDOT:PSS as a counter-electrode material for DSSCs in this setup.

To assess the charge transfer efficiency and recombination dynamics of each counter electrode (Pt, PEDOT:PSS, and graphene), *J-V* measurements under varying light intensities (such as 7.8, 27.2, 68.4, and 102.9 $mWcm^{-2}$) were also conducted (Figure 4(b-d), Table 4). The PEDOT:PSS-based DSSCs exhibit lower J_{SC} than Pt and graphene electrodes at all intensities. The *J-V* curves show a noticeable s-shape, especially under high light intensities, resulting in a drop of FF from 55.2% to 25.5% (from the intensity of 7.8 to 102.9 $mWcm^{-2}$), which is associated with higher series resistance or slower charge transfer kinetics. The J_{SC} values of DSSCs with a Pt counter electrode increase with light intensity, while the FF decreases, leading to a

TABLE 3
PERFORMANCE OF DSSCS WITH DIFFERENT CES (PT, PEDOT:PSS, AND GRAPHENE) AND CELLS AT ~100 $MW.CM^{-2}$ (1 SUN EQUIVALENT) INCLUDING THEIR AVERAGES (AVG)

CE	Cell	V_{OC} (V)	J_{SC} (mA. cm^{-2})	FF (%)	PCE (%)
Pt	C1	0.67	12.8	51.5	4.36
	C2	0.69	12.0	48.1	3.80
	C3	0.68	12.3	48.6	3.95
	Avg	***0.68±0.01***	***12.4±0.40***	***49.4±1.8***	***4.0±0.29***
PEDOT:PSS	C1	0.68	4.4	25.5	0.75
	C2	0.66	5.0	27.4	0.87
	C3	0.66	4.6	25.8	0.77
	Avg	***0.67±0.01***	***4.7±0.31***	***26.2±1.0***	***0.8±0.06***
Graphene	C1	0.68	15.1	51.1	5.12
	C2	0.66	15.5	52.5	5.23
	C3	0.64	11.9	55.3	4.09
	Avg	***0.66±0.02***	***14.2±1.97***	***53.0±2.1***	***4.81±0.6***

maximum PCE of 5.34% at 27.2 mW. cm^{-2} of intensity value. The FF remains relatively stable, around 54-69%, indicating consistent charge transfer and minimal resistive losses at higher intensities [18]. The DSSCs with graphene counter electrodes achieve the highest performance across all light intensities. It shows stable open-circuit voltage (V_{OC}) values and smooth *J-V* curves across intensities, suggesting that graphene is highly effective in facilitating current generation and supporting high efficiency across a range of illumination intensities.

Charge carrier recombination can be characterized from the light intensity dependence measurements (Figure 4(b-d)), examining V_{OC} and J_{SC} inferred from *J-V* curves as a function of light intensity [19-21]. Figure 5a shows the V_{OC} as a function of the light intensity of the DSSCs with different counter electrodes. The slope *s* (where $V_{OC} \propto s \cdot \log(I_{light})$) should approach 1 when radiative processes dominate recombination. When trap-assisted recombination or non-radiative recombination dominates, the slope *s* is larger than 1 [19, 22, 23]. Devices based on Pt as a counter electrode show the highest slope, indicating that trap-assisted recombination is more prominent. PEDOT:PSS and graphene-based DSSCs show lower trap-assisted recombination. Note also that the fitting was taken starting from the light intensity of 38.1 mW.cm^{-2} as lower intensity seems to have a steeper slope.

Figure 5(b) shows the J_{SC} as a function of light intensity of the DSSCs with different counter electrodes. Generally, the relationship between J_{SC} and incident light intensity is expressed as $J_{SC} \propto I^{\alpha}$, where $\alpha = 1$ indicates that all dissociated free carriers are collected before recombination, and $\alpha < 1$ suggests that J_{SC} is influenced by bimolecular recombination, meaning most carriers are extracted before recombining [19, 21]. The bimolecular recombination in DSSCs possibly occurs between electrons in the conduction band of the TiO_2 and the triiodide ion (I_3^-) in the electrolyte (process C shown in Figure 1(b)) [24]. Both Pt- and graphene-based DSSCs do not significantly suffer from bimolecular recombination, while the much smaller α (~0.29) found in PEDOT:PSS-based DSSCs indicates that the much smaller J_{SC} and FF in PEDOT:PSS devices are due to the bimolecular recombination.

TABLE 4
PERFORMANCE OF DSSCS WITH DIFFERENT CES AND DIFFERENT INTENSITIES FOR ONE OF THE CELL (C1)

CE	Intensity (mW.cm^{-2})	V_{OC} (V)	J_{SC} (mA.cm^{-2})	FF (%)	PCE (%)
Pt	7.8	0.56	0.45	69.6	2.24
	27.2	0.64	3.54	64.2	5.34
	47.8	0.64	6.33	60.8	5.16
	68.4	0.66	8.77	56.6	4.79
	85.6	0.66	10.9	54.8	4.61
	102.9	0.68	12.8	51.5	4.36
PEDOT:PSS	7.8	0.56	0.42	55.2	1.67
	27.2	0.64	3.00	26.3	1.86
	47.8	0.66	3.74	24.8	1.28
	68.4	0.66	4.05	25.4	0.99
	85.6	0.66	4.25	25.9	0.85
	102.9	0.68	4.44	25.5	0.75
Graphene	7.8	0.56	0.54	63.7	2.47
	27.2	0.64	4.24	64.2	6.40
	47.8	0.66	7.51	60.0	6.23
	68.4	0.68	10.37	55.7	5.74
	85.6	0.68	12.90	53.3	5.46
	102.9	0.68	15.14	51.1	5.12

To understand the differences in charge extraction losses caused by bimolecular recombination, we conducted charge extraction measurements under both open-circuit and short-circuit conditions [25-27]. Figure 5(c) shows the Q_{OC} versus V_{OC} of the cells with different counter electrodes as a function of light intensity. Q_{OC} is charged extraction measured in open circuit conditions [25, 27]. All three materials show a similar upward trend of extracted charge with increasing V_{OC} (measured at open-circuit conditions). Still, graphene generates slightly more charge for a given voltage than PEDOT:PSS. Figure 5(d) shows the Q_{SC} versus J_{SC} of the cells with different counter electrodes as a function of light intensity. Q_{SC} is charge extraction measured in circuit condition [27]. Pt and graphene show more consistent behavior across the entire range. PEDOT:PSS may store more charge during short-circuit conditions, possibly indicating a higher capacitance due to the lower charge transfer efficiency of the PEDOT:PSS layer

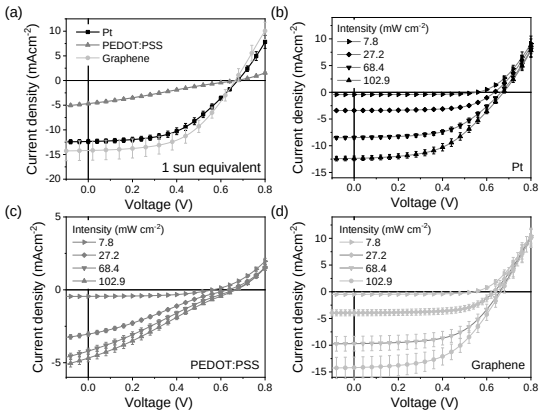

Figure 4. Average *J-V* curves of (a) the cells with a light intensity equivalent to one sun, and *J-V* curves of DSSCs under different light intensities and for (b) Pt, (c) PEDOT:PSS, and (d) graphene-based electrodes.

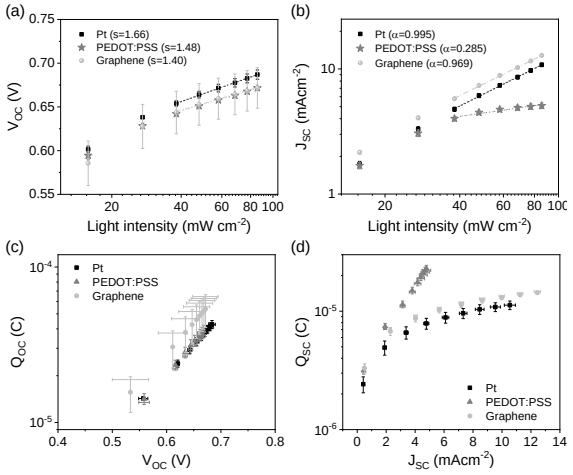

Figure 5. (a) V_{OC} and (b) J_{SC} versus light intensity for DSSCs with different counter electrodes. (c) Q_{OC} versus V_{OC} and (d) Q_{SC} versus J_{SC} as derived from the *J-V* vs light intensity measurements.

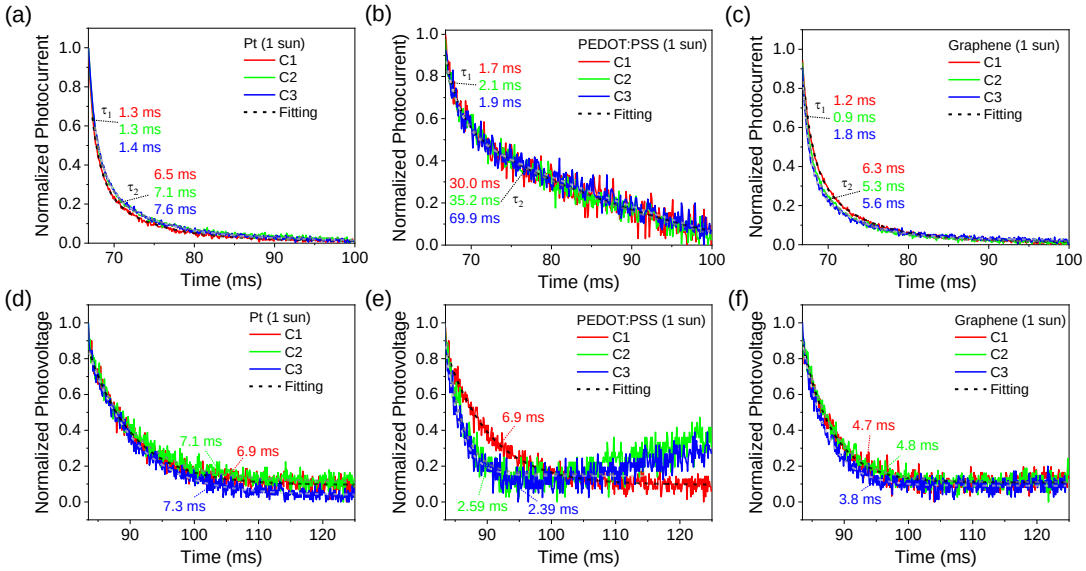

Figure 6. Normalized photocurrent decays of (a) Pt, (b) PEDOT:PSS, and (c) graphene-based DSSCs; Normalized photovoltage decays of (d) Pt, (e) PEDOT:PSS, and (f) graphene-based DSSCs of different cells (C1, C2, C3) measured at a light intensity equivalent to 1 sun.

compared to Pt and graphene. The high charge generation could not be efficiently extracted, leading to a higher extracted current despite having the same J_{SC} level as Pt and graphene-based DSSCs (Figure 5(d)).

Further insights into charge recombination across the DSSCs can be inferred from transient photovoltage (TPV) and transient photocurrent (TPC) measurements [27]. The measurements were conducted using a slow modulation frequency (2–7 Hz repetition) to measure electron lifetime and electron transport time. The TPCs were measured for DSSCs at short circuit conditions for different counter electrodes. Figure 6 (a-c) shows normalized photocurrent versus time of the cells. The photocurrent of C1, C2, and C3 represent different cells but under the same conditions (same counter electrodes and illumination). The fact that the normalized photocurrent decay curves are similar across C1, C2, and C3 for all counter electrodes suggests a reasonable level of reproducibility in our experiments. The photocurrent decays could only be well-fitted using the bi-exponential function, as shown in (2):

$$J_{SC} = A_1 e^{\left(-\frac{t}{\tau_{tr1}}\right)} + A_2 e^{\left(-\frac{t}{\tau_{tr2}}\right)} + B \quad (2)$$

where A and B are constants, t is decay time, and τ_{tr} is electron transport time.

The photocurrent decay times could be attributed to transport time in DSSCs. As the fast components of the transport time (1-2 ms) are quite similar for devices with different counter electrodes, it might be attributed to the electron transport in the photoanode (TiO_2). The timescale of this transport time agrees with the energy diagram shown in Figure 1(b) (process 3). The main difference in the photocurrent decay is in the slower component. This component is probably related to the catalytic activity in the counter electrode and electron transport to I_3^- [27]. For Pt-based DSSCs, the transport time in counter electrode and electrolyte is 7 ms, slightly slower than the transport time for graphene-based DSSCs (~6 ms). The transport time in PEDOT:PSS DSSCs is 6-7 times slower than the other two counterparts, suggesting less efficient charge collection due to the slow dye regeneration and the build-up of I_3^-.

Figure 6 (d-f) shows normalized photovoltage versus time of the cells. The electron lifetime can be inferred from the photovoltage decay of the TPV measurements. The photovoltage decay of DSSCs with different counter electrodes is well-fitted using the mono-exponential function, as shown in (3) [19].

$$V_{OC} = Ae^{\left(-\frac{t}{\tau_e}\right)} + B \quad (3)$$

Where A and B are constants, t is decay time, whereas τ_e is electron transport time.

The electron lifetime refers to the average time an electron remains in the conduction band before recombining with a hole [19]. It provides insight into the recombination dynamics in the material. A faster lifetime implies faster recombination (most probably recombination from the electron in TiO_2 to I_3^- in the electrolyte). The TPV reflects the recombination of electrons at the TiO_2 and electrolyte interface. The electron lifetime in Pt-based DSSC is ~7 ms, while its decrease becomes ~4 ms for graphene-based DSSC. The two cells with PEDOT:PSS counter electrode exhibit the shortest lifetime (~2.5 ms) compared to the other two counter electrodes. This is in agreement with the trend in bimolecular recombination in DSSCs inferred from Figure 5(b).

IV. Conclusion

In conclusion, it has been demonstrated that DSSCs with graphene-based counter electrodes outperform those with Pt and PEDOT:PSS in terms of photocurrent and PCE, mainly due to their superior charge extraction characteristics. As a result, graphene-based DSSCs achieve the highest photocurrent density (J_{SC}) up to 15.5 $mA.cm^{-2}$ and power conversion efficiency (PCE) up to 5.23% at an intensity equivalent to 1 sun (around 100 $mWcm^{-2}$). This is supported by various characterizations,

including light intensity-dependent *J-V* curves and charge extraction at different voltage bias conditions (open circuit and short circuit conditions), which show minimal bimolecular recombination and efficient charge collection at short-circuit conditions (Q_{SC}). In contrast, PEDOT:PSS-based DSSC exhibited lower charge transfer efficiency, leading to higher resistive losses and poor current generation. TPC and TPV measurements also reveal that the PEDOT:PSS-based DSSCs exhibited the slowest charge transport and shortest electron lifetime compared to the DSSCs with Pt and graphene counter electrodes. The findings emphasize the importance of optimizing counter-electrode materials for efficient charge extraction and reduced recombination in DSSC devices.

DECLARATIONS

Conflict of Interest

The authors have declared that no competing interests exist.

CRediT Authorship Contribution

Evi Nur Azizah: Investigation, Data curation; Nunik Nurhayati: Investigation, Writing-Original Draft; Lalu Jihad Al Jazeera: Investigation, Data curation; Lia Yuliantini: Investigation, Data Curation; Mohammad Hatta: Data curation, Analysis; Tahta Amrillah: Investigation, Data curation ;Natalita Maulani Nursam: Writing-Reviewing, Funding Acquistion; Yuliar Firdaus: Conceptualization, Supervision, Analysis, Visualization, Writing-Reviewing and Editing, Funding Acquisition.

Funding

This research is fully funded by Riset dan Inovasi untuk Indonesia Maju (RIIM) Number 82/II.7/HK/2022.

Acknowledgment

The authors thankfully acknowledge the support of the Advanced Photovoltaic and Functional Electronic Devices research group at the Research Center for Electronics, Badan Riset dan Inovasi Nasional (BRIN). E-layanan Sains (ELSA) BRIN is acknowledged for providing access to the materials characterization.

REFERENCES

[1] A. Hagfeldt, G. Boschloo, L. Sun, L. Kloo, and H. Pettersson, "Dye-Sensitized Solar Cells," *Chem. Rev.*, vol. 110, no. 11, pp. 6595–6663, Nov. 2010, doi: 10.1021/cr900356p.

[2] S. Yoon, S. Tak, J. Kim, Y. Jun, K. Kang, and J. Park, "Application of transparent dye-sensitized solar cells to building integrated photovoltaic systems," *Build. Environ.*, vol. 46, no. 10, pp. 1899–1904, Oct. 2011, doi: 10.1016/j.buildenv.2011.03.010.

[3] Z. Wen *et al.*, "Self-powered textile for wearable electronics by hybridizing fiber-shaped nanogenerators, solar cells, and supercapacitors," *Sci. Adv.*, vol. 2, no. 10, Oct 2016, Art. no. e1600097, doi: 10.1126/sciadv.1600097.

[4] J. Wu *et al.*, "Counter electrodes in dye-sensitized solar cells," *Chem. Soc. Rev.*, vol. 46, no. 19, pp. 5975–6023, Aug. 2017, doi: 10.1039/C6CS00752J.

[5] S. Thomas, T. G. Deepak, G. S. Anjusree, T. A. Arun, S. V. Nair, and A. S. Nair, "A review on counter electrode materials in dye-sensitized solar cells," *J. Mater. Chem. A*, vol. 2, no. 13, pp. 4474–4490, Nov. 2014, doi: 10.1039/C3TA13374E.

[6] H. Murata, Y. Nakajima, N. Saitoh, N. Yoshizawa, T. Suemasu, and K. Toko, "High-electrical-conductivity multilayer graphene formed by layer exchange with controlled thickness and interlayer," *Sci. Rep.*, vol. 9, no. 1, Mar. 2019, Art. no. 4068, doi: 10.1038/s41598-019-40547-0.

[7] A. Peigney, C. Laurent, E. Flahaut, R. R. Bacsa, and A. Rousset, "Specific surface area of carbon nanotubes and bundles of carbon nanotubes," *Carbon*, vol. 39, no. 4, pp. 507–514, Apr. 2001, doi: 10.1016/S0008-6223(00)00155-X.

[8] P. Z. Sun *et al.*, "Unexpected catalytic activity of nanorippled graphene," *Proc. Natl. Acad. Sci.*, vol. 120, no. 12, Mar. 2023, Art. no. e2300481120, doi: 10.1073/pnas.2300481120

[9] T. Yohannes and O. Inganäs, "Photoelectrochemical studies of the junction between poly[3-(4-octylphenyl)thiophene] and a redox polymer electrolyte," *Sol. Energy Mater. Sol. Cells*, vol. 51, no. 2, pp. 193–202, Feb. 1998, doi: 10.1016/S0927-0248(97)00213-4.

[10] Y. Ren *et al.*, "Hydroxamic acid pre-adsorption raises the efficiency of cosensitized solar cells," *Nat.*, vol. 613 pp. 60–65, Jan. 2023, doi: 10.1038/s41586-022-05460-z.

[11] E. S. Nurazizah, A. Aprilia, R. Risdiana, and L. Safriani, "Different roles between PEDOT:PSS as counter electrode and PEDOT:carrageenan as electrolyte in dye-sensitized Solar cell applications: a systematic literature review," *Polym.*, vol. 15, no. 12, Jun. 2023, Art. no. 2725, doi: 10.3390/polym15122725.

[12] K. K. Putra, E. S. Rosa, Shobih, and N. Prastomo, "Development of monolithic dye sensitized solar cell fabrication with polymer-based counter electrode," *J. Phys. Conf. Ser.*, vol. 1191, no. 1, Mar. 2019,Art. no. 012029, doi: 10.1088/1742-6596/1191/1/012029.

[13] S.-H. Park, J.-U. Kim, J.-K. Lee, and M.-R. Kim, "Photovoltaic properties of dye-sensitized solar cells with thermal treated PEDOT:PSS as counter electrodes," *Mol. Cryst. Liq. Cryst.*, vol. 471, no. 1, pp. 113–121, Sept. 2007, doi: 10.1080/15421400701545437.

[14] W. Maiaugree *et al.*, "A dye sensitized solar cell using natural counter electrode and natural dye derived from mangosteen peel waste," *Sci. Rep.*, vol. 5, no. 1, Oct. 2015, , Art. no. 15230, doi: 10.1038/srep15230.

[15] N. Fuke *et al.*, "Influence of $TiCl_4$ treatment on back contact dye-sensitized solar cells sensitized with black dye," *Energy Environ. Sci.*, vol. 2, no. 11, pp. 1205–1209, Jul. 2009, doi: 10.1039/B909689B.

[16] H. Wang and Y. H. Hu, "Graphene as a counter electrode material for dye-sensitized solar cells," *Energy Environ, Sci.*, vol. 5, no. 8, pp. 8182–8188, Jun. 2012, doi: 10.1039/C2EE21905K.

[17] K. Sim, S.-J. Sung, S.-N. Park, D.-H. Kim, and J.-K. Kang, "Particulate counter electrode system for enhanced light harvesting in dye-sensitized solar cells," *Opt. Mater. Express*, vol. 3, no. 6, pp. 739–746, Jun. 2013, doi: 10.1364/OME.3.000739.

[18] J. H. Kim, K. J. Moon, J. M. Kim, D. Lee, and S. H. Kim, "Effects of various light-intensity and temperature environments on the photovoltaic performance of dye-sensitized solar cells," *Sol. Energy*, vol. 113, pp. 251–257, Mar. 2015.

[19] Y. Firdaus *et al.*, "Polymer main-chain substitution effects on the efficiency of nonfullerene BHJ solar cells," *Adv. Energy Mater.*, vol. 7, no. 21, Nov. 2017, Art. no. 1700834, doi: 10.1002/aenm.201700834.

[20] Y. Firdaus, Q. He, L. Muliani, E. S. Rosa, M. Heeney, and T. D. Anthopoulos, "Charge transport and recombination in wide-bandgap Y6 derivatives-based organic solar cells," *Adv. Nat. Sci.: Nanosci. Nanotechnol.*, vol. 13, no. 2, May 2022, Art. no. 025001, doi: 10.1088/2043-6262/ac6c23.

[21] R.-Z. Liang *et al.*, "Additive-morphology interplay and loss channels in "all-small-molecule" bulk-heterojunction (BHJ) solar cells with the nonfullerene acceptor IDTTBM," *Adv. Funct. Mater.*, vol. 28, no. 7, Feb. 2018, Art. no. 1705464, doi: 10.1002/adfm.201705464.

[22] L. J. A. Koster, V. D. Mihailetchi, R. Ramaker, and P. W. M. Blom, "Light intensity dependence of open-circuit voltage of polymer:fullerene solar cells," *Appl. Phys. Lett.*, vol. 86, no. 12, Mar. 2005, Art. no. 123509, doi: 10.1063/1.1889240.

[23] S. Ryu, N. Y. Ha, Y. H. Ahn, J.-Y. Park, and S. Lee, "Light intensity dependence of organic solar cell operation and dominance switching between Shockley–Read–Hall and bimolecular recombination losses," *Sci. Rep.*, vol. 11, no. 1, Aug. 2021, Art. no. 16781, doi: 10.1038/s41598-021-96222-w.

[24] H. Paulsson, L. Kloo, A. Hagfeldt, and G. Boschloo, "Electron transport and recombination in dye-sensitized solar cells with ionic liquid electrolytes," *J. Electroanal. Chem.*, vol. 586, no. 1, pp. 56–61, Jan. 2006, doi: 10.1016/j.jelechem.2005.09.011.

[25] Y. Hao *et al.*, "A small electron donor in cobalt complex electrolyte significantly improves efficiency in dye-sensitized solar cells," *Nat. Commun.*, vol. 7, no. 1, Dec. 2016, Art. no. 13934, doi: 10.1038/ncomms13934.

[26] Y. Firdaus *et al.*, "Novel wide-bandgap non-fullerene acceptors for efficient tandem organic solar cells," *J. Mater. Chem. A*, vol. 8, no. 3, pp. 1164–1175, Dec. 2020, doi: 10.1039/C9TA11752K

[27] G. Boschloo, L. Häggman, and A. Hagfeldt, "Quantification of the effect of 4-tert-butylpyridine addition to I^-/I^{3-} redox electrolytes in dye-sensitized nanostructured TiO_2 solar cells," *J. Phys. Chem. B*, vol. 110, no. 26, pp. 13144–13150, Jul. 2006, doi: 10.1021/jp0619641.